The effect of adding a magnetic oxide in the grain boundaries of HAMR media

Bing Zhou, B. S. D. Ch. S. Varaprasad, Zhengkun Dai, David E. Laughlin, and Jian-Gang Zhu

Citation: Appl. Phys. Lett. **113**, 082401 (2018); doi: 10.1063/1.5037171
View online: https://doi.org/10.1063/1.5037171
View Table of Contents: http://aip.scitation.org/toc/apl/113/8
Published by the American Institute of Physics

The effect of adding a magnetic oxide in the grain boundaries of HAMR media

Bing Zhou,[1,2,a)] B. S. D. Ch. S. Varaprasad,[1,3] Zhengkun Dai,[1,3] David E. Laughlin,[1,2,3] and Jian-Gang Zhu[1,2,3]
[1]*Data Storage Systems Center, Carnegie Mellon University, Pittsburgh, Pennsylvania 15213, USA*
[2]*Materials Science and Engineering Department, Carnegie Mellon University, Pittsburgh, Pennsylvania 15213, USA*
[3]*Electrical and Computer Engineering Department, Carnegie Mellon University, Pittsburgh, Pennsylvania 15213, USA*

(Received 21 April 2018; accepted 3 August 2018; published online 21 August 2018)

Grain-to-grain Curie temperature (T_c) variation in media reduces the signal-to-noise ratio due to its contribution to the transition jitter noise, especially when the average grain size is decreased to increase the area storage capacity. Thermally insulating magnetic grain boundaries may suppress such grain-to-grain T_c variation, especially at small grain sizes. In this paper, we discuss the effect of adding a thermally insulating magnetic oxide, in particular, $BaFe_xO_y$, to the grain boundaries of granular FePt-C heat-assisted magnetic recording media. It is found that $BaFe_xO_y$ is chemically inert with respect to FePt and the chemical ordering of FePt-$BaFe_xO_y$-C media is similar to that of FePt-C media. By tuning the volume fraction of $BaFe_xO_y$ and C, well-separated FePt grains (average grain size = 6.8 nm) surrounded by $BaFe_xO_y$ shells enable the attainment of perpendicular H_c greater than 35 kOe. Chemical mapping by transition electron microscopy shows that the magnetic oxide appears to be crystalline and completely surrounds the FePt grains. Temperature-dependent magnetization measurements indicate an effective increase in the magnetic grain size at temperatures below the FePt Curie temperature. The pulsed laser pump-probe measurement indicates a measurable reduction of the Curie temperature variation for the FePt-$BaFe_xO_y$-C media compared to the reference FePt-C media. *Published by AIP Publishing.* https://doi.org/10.1063/1.5037171

FePt-C granular film structures have been considered as the most promising candidates for heat-assisted magnetic recording (HAMR) media due to the large magnetocrystalline anisotropy of $L1_0$ FePt with $K_u > 7 \times 10^7$ erg/cc.[1,2] During a recording process of HAMR media, a transition region is determined when the medium is cooled from the Curie temperature to the temperature below where the anisotropy field becomes larger than the local head field. Grain-to-grain variation of T_c, therefore, will directly translate into a transition position jitter and can yield a significant degradation signal-to-noise ratio (SNR), limiting the recording area density capability.[3–5]

The origin of the grain-to-grain Curie temperature variation arises from the following: For a FePt grain, the ferromagnetic exchange fields of the surface spins are significantly smaller than those of the spins in the core. When the grain size becomes less than about 8 nm, the Curie temperature of the FePt grains starts to decrease with the reducing grain size due to the increase in the surface-to-volume ratio. The resulting grain size dependence of the grain Curie temperature gives rise to a Curie temperature distribution for a finite grain size distribution in the media.[6–9] The grain size dependence of the Curie temperature becomes more pronounced at smaller grain sizes, which is counter to the desire to reduce the grain size to increase the recording area density capability for HAMR technology.

One way to mitigate the Curie temperature dependence on the grain size is to produce the FePt-$L1_0$ grains with magnetic grain boundaries with a Curie temperature greater than that of FePt grains. The magnetic grain boundary material should be thermally insulating to prevent lateral heat transfer, thus maintaining a sufficient lateral thermal gradient in the magnetic medium layer during the recording processes.

In this paper, we propose a thermal-insulating magnetic oxide as part of grain boundary material for reducing grain-to-grain T_c variation. In particular, we report on an experimental study of mixing $BaFe_xO_y$ with C as the grain boundary material. The possibility of utilizing $BaFe_{12}O_{19}$ was explored in this study, since $BaFe_{12}O_{19}$ is a ferrimagnetic material with high Curie temperature (can be >800 K)[10] and relatively low thermal conductivity 4 W m^{-1} K^{-1}.[11]

Films were sputtered on thermally grown SiO_2 substrates using an AJA system with a base pressure less than 2×10^{-9} Torr. Two series of samples C1-C3 and T1-T2 with film stack Si | SiO_2 | Ta (5 nm) | Cr (100 nm) | MgO (9 nm) | magnetic media (M) (7.5 nm) were prepared. All samples have the same layer structure up to the MgO layer. In the first series of samples, the media layer M is FePt + X vol. % C, where X = 30, 32, and 35, for C1, C2, and C3, respectively. In the second series of samples, the media layer M is FePt + X vol. % (C + $BaFe_xO_y$), where X = 40 and 42, for T1 and T2, respectively. The Ta and Cr layers were DC sputtered at a pressure of 5 mTorr at room temperature and 200 °C, respectively. They were subsequently annealed in vacuum at 650 °C for 40 min. The Cr buffer layer is used to obtain large MgO

a)Author to whom correspondence should be addressed: bingzhou@andrew.cmu.edu

grains with a strong (002) texture and to serve as a heat sink. The MgO layer was RF sputtered at 10 mTorr at room temperature. The sample was then preheated at 650 °C for 30 min to stabilize the deposition temperature of media layer M. The FePt alloy target and the C target were subsequently DC sputtered with the RF-sputtered $BaFe_{12}O_{19}$ target onto the predeposited MgO at 5 mTorr at 650 °C. The crystalline texture and degree of chemical ordering were analyzed and determined from X-ray diffraction spectra using Cu Kα radiation. The microstructure and chemical mapping of various samples were studied by bright-field transmission electron microscopy (TEM) imaging, high-resolution TEM imaging (HR-TEM), scanning TEM high angle annular dark field imaging (STEM-HAADF), and STEM energy dispersive x-ray spectroscopy (STEM-EDS). The FePt grain size analysis of all samples was examined from multiple regions of each sample imaged by bright-field TEM. The room temperature magnetic properties and the saturation remanence (M_r) vs. temperature (T) behavior of all samples were examined using the Quantum Design's Magnetic Property Measurement System (MPMS 3) with a maximum field of 7 T. During the M vs. T measurements, the samples were arranged perpendicular to the magnetic field direction. All samples were saturated at 7 T prior to performing the measurements at elevated temperatures from 300 K to 700 K at zero field. The T_c distribution of all samples was measured by a pump probe setup based on the thermal remanence after pulse laser heating. The experimental set-up of the σT_c measurement is mentioned in a previous publication with several modifications.[12] Compared with the previous setup, the pulse width was reduced from ~12 ns to ~0.7 ns, which further eliminates the effect of dwell times at high temperatures. The pump beam and probe beam were combined and focused by a 10× objective lens, which further reduced the spot size. Each pulse energy was independently measured using a pulse energy meter. The measured σT_c of each sample was averaged from the fittings of five measurements at different locations.

Figure 1(a) shows the XRD patterns of C1-C3 and T1-T2, with the MgO and FePt peaks indexed. The peak at $2\theta = 43°$ corresponds to MgO (002) and there are no other MgO peaks observed, suggesting that strong (002)-textured thin films were obtained. All samples show only FePt (001) and FePt (002) peaks, indicating a well-textured FePt growth on the MgO with and without $BaFe_xO_y$. The large integrated intensity ratio between the super lattice peak FePt (001) and the fundamental peak FePt (002) in all samples demonstrates good chemical ordering in $L1_0$ FePt. The order parameter (S), shown in Fig. 1(b), was calculated from the ratio of I_{001}/I_{002} with the absorption factor and Lorentz factor taken into account, where I_{001} and I_{002} are integrated intensities of FePt (001) and (002) peaks, respectively.[13] S is plotted against the mean grain size of all samples, which was obtained from the in-plane bright field TEM images shown later. In the first series of samples, C1-C3 (represented by solid squares), S shows a decreasing trend, when the carbon volume percentage increases from 30 to 35. This is due to grain size reduction causing an increasing surface to volume ratio of the FePt grains as the carbon volume percentage increases. S of the second series of samples, T1 and T2 (represented by open squares), generally follows the same trend as that shown in C1-C3. The chemical ordering of FePt remains constant with $BaFe_xO_y$ additions to the media layer, suggesting that FePt is chemically inert to $BaFe_xO_y$.

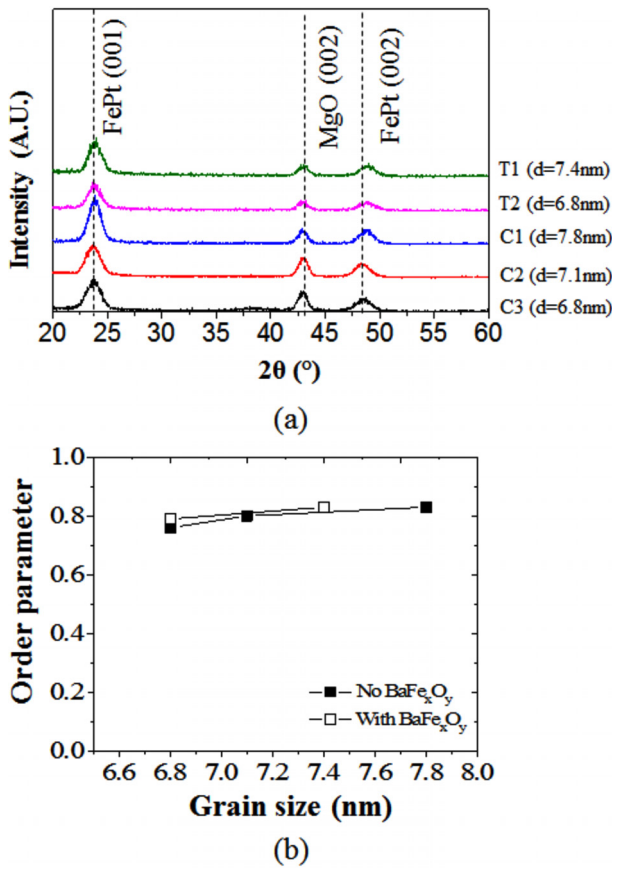

FIG. 1. (a) XRD patterns of film stack Si | SiO_2 | Ta (5 nm) | Cr (100 nm) | MgO(9 nm) | M (7.5 nm) with the M layer being FePt-X vol. % C (X = 30, 32, and 35 for C1, C2, and C3) or FePt-X vol. % (C + $BaFe_xO_y$) (X = 40 and 42 for T1 and T2); (b) chemical order parameter (S) of C1-C3 and T1-T2 as a function of the average grain size.

Figures 2(a) and 2(b) show the typical perpendicular and in-plane M-H loops for samples with (T2) and without $BaFe_xO_y$ (C3), taken at room temperature. The samples have a similar average grain size of 6.8 nm. All samples show high perpendicular coercivity ranging from 38 kOe to 42 kOe, suggesting good $L1_0$ ordering of FePt films with and without $BaFe_xO_y$. The in-plane M-H loops of all samples show a small opening with coercivity <7 kOe and normalized remanence magnetization <0.14, indicating that the c-axis of the FePt film is predominantly perpendicular to the film plane. Both the perpendicular and in-plane magnetic

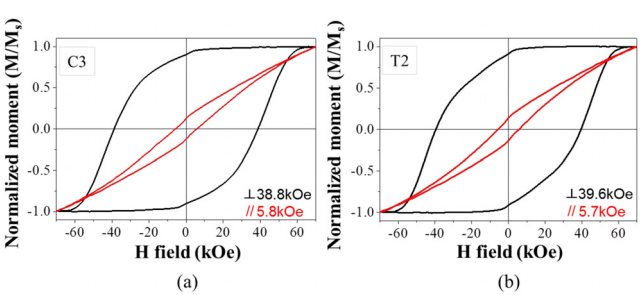

FIG. 2. Room temperature in-plane and perpendicular hysteresis loops for (a) C3 and (b) T2.

behaviors are consistent with the XRD results shown in Fig. 1. Note that the coercivity and squareness of the perpendicular M-H loop of samples C3 and T2 are similar, so it can be inferred that $BaFe_xO_y$ in the media layer does not strongly exchange couple the adjacent FePt grains nor destroy the microstructure.

Figures 3(a), 3(b), 3(d), and 3(e) show the in-plane bright field TEM images of C1, C3, T1, and T2. The in-plane bright field TEM image of C2 is not shown here. All samples show a well-separated granular microstructure. The grain size analysis was performed on multiple regions from each sample to ensure the accuracy. Our analysis shows that the mean grain size of FePt decreases gradually from 7.8 nm to 6.8 nm as the volume fraction of the grain boundary material (C) increases from 30 vol. % to 35 vol. % in samples C1 to C3. Our analysis also shows that from T1 to T2, the grain size of FePt decreases gradually from 7.4 nm to 6.8 nm as the volume fraction of grain boundary materials ($C + BaFe_xO_y$) increases from 40 vol. % to 42 vol. % of the total media layer. The in-plane microstructure of 7.5 nm FePt-30 vol. % $BaFe_xO_y$ was also examined (result not shown), and it shows an interconnected microstructure similar to other oxides such as SiO_2 and TiO_2 shown in the previous literature.[14] Therefore, the C content is crucial to control the microstructure. Figures 3(c) and 3(f) show the HR-TEM images for C1 and T1, respectively. It is observed that the FePt grains are enclosed with graphitic regions followed by amorphous carbon, whereas for FePt-$BaFe_xO_y$-C media, connecting crystalline shells are found around the FePt grains. To find where $BaFe_xO_y$ resides in the media layer, elemental mapping of Fe, Pt, and O was performed on the samples with $BaFe_xO_y$. The elemental mapping of Ba is not used in this study, since the overall atomic percentage of Ba is too low to be detected. Figures 3(g)–3(k) show the HAADF-STEM and EDS mappings of Fe and Pt of the FePt-$BaFe_xO_y$-C media, T2. The chemical mapping of Pt shows the well-defined grains as FePt grains, which suggests that the Pt is only in the FePt grains. This is consistent with the HAADF-STEM images. The chemical mapping of Fe shows that Fe exists not only in FePt grains but also in the grain boundary. Figures 3(j) and 3(k) show the overlapped EDS mappings of Fe-Pt and Pt-O. This clearly indicates that the crystalline shell surrounding FePt grains shown in HR-TEM images contains a significant amount of Fe and O. Therefore, it can be concluded that $BaFe_xO_y$ added in the media layer forms a crystalline shell surrounding FePt grains and the shells are connected with each other. However, although $BaFe_xO_y$ shells formed around FePt grains are physically connected, the FePt grains are still magnetically decoupled from each other, since the room temperature perpendicular H_c, shown in Fig. 2, is comparable for the cases with and without $BaFe_xO_y$ for similar mean grain size media. Based on the XRD patterns, the room temperature magnetic properties, and the microstructure analysis, it can be concluded that $BaFe_xO_y$ added in the media layer forms a crystalline shell surrounding FePt grains and it does not chemically interact with FePt nor strongly exchange couple the adjacent FePt grains.

In the M vs. T measurements, the change in the remanent magnetization (M_r) was measured when temperature increased from 300 K to 700 K. As the temperature increases, some of the FePt grains become super-paramagnetic, and thus, M_r decreases. At a certain temperature (T_c*), M_r drops

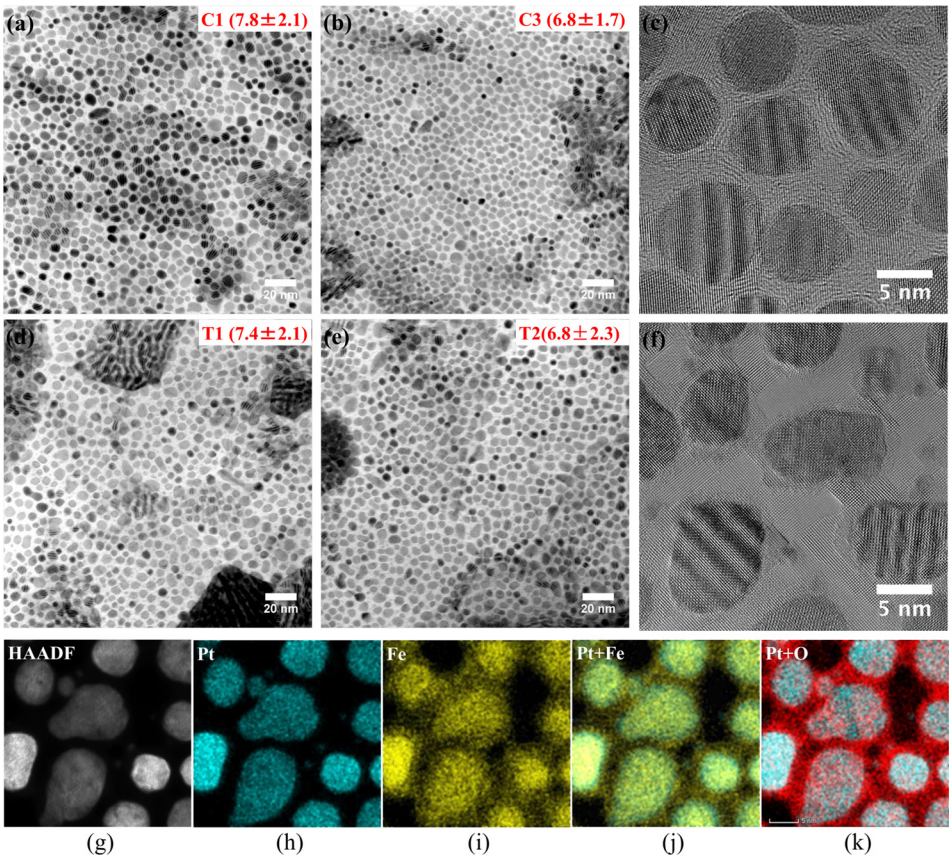

FIG. 3. The in-plane bright-field TEM micrographs for (a) C1, (b) C3, (d) T1, and (e) T2 with the insets being their corresponding average grain size and standard deviation; HR-TEM micrographs for (c) C1 (FePt-30 vol. % C) and (f) T1 [FePt-40 vol. % ($C + BaFe_xO_y$)]; HAADF-STEM micrographs (g) and the EDS mapping of (h) Pt, (i) Fe, (j) Pt + Fe, and (k) Pt + O of T1 [FePt-40 vol. % ($C + BaFe_xO_y$)].

to zero as all grains have become super-paramagnetic. Figure 4(a) shows the comparison of the normalized M_r vs. T behavior between FePt-C media and FePt-$BaFe_xO_y$-C media. Note that M_r at different temperatures has been normalized with respect to its room temperature M_r for each sample. Therefore, the moment contribution from the grain boundary has also been included in the measurements. The red and black triangles represent the M_r vs. T behavior for FePt-C media with grain sizes of 7.8 nm (C1) and 6.8 nm (C3), whereas the green squares and blue circles represent FePt-$BaFe_xO_y$-C with grain sizes of 7.4 nm (T1) and 6.8 nm (T2). In the FePt-C media, the normalized M_r vs. T curve of the sample with the larger grain size (C1) shifts rightward toward the higher temperature region compared with that of the sample with a smaller grain size (C3), primarily due to the finite size effect and surface effect. Comparing C3 and T2, it is evident that the addition of $BaFe_xO_y$ in the media layer shifts the normalized M_r vs T curve towards higher temperature with the same FePt grain size. Since the M_r vs. T curves of C1 and T1 are similar to each other, this shows that the effect of adding $BaFe_xO_y$ in the media layer corresponds to a 5% increase in the magnetic grain size with the pure C grain boundary. This enhancement of M_r at elevated temperature is due to the magnetic crystalline shell of $BaFe_xO_y$ formed around the FePt grains, since the magnetic spins in the shell region are weakly exchange coupled with the surface atomic spins of FePt grains which promotes their spin coherence with those in the FePt core. As a result, the surface atomic spins of FePt at the grain/magnetic grain boundary interface can maintain their spin coherence to a higher temperature compared with the case of the grain/non-magnetic grain boundary, such as FePt-C media. The exchange coupling between $BaFe_xO_y$ and FePt is weak enough so that the FePt grains are magnetically independent under magnetic field (shown in perpendicular hysteresis loops in Fig. 2) but strong enough to alleviate the FePt surface spin incoherence at the grain/grain boundary interface.

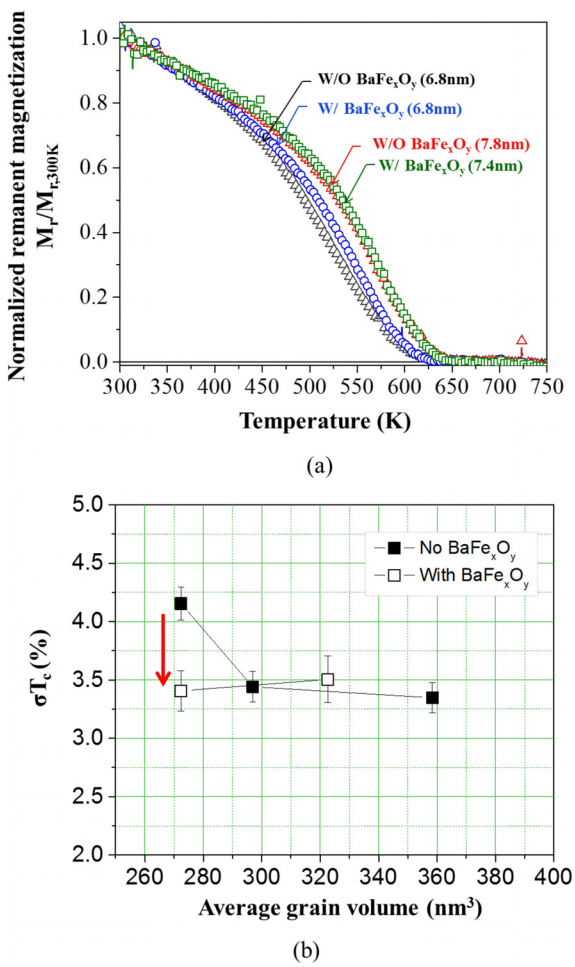

FIG. 4. (a) Experimental normalized M_r vs. T curve for C1 (red triangle), C3 (black triangle), T1 (green square), and T2 (blue circle); (b) Curie temperature distribution σT_C as a function of average grain volume for FePt-C and FePt-$BaFe_xO_y$-C media.

Figure 4(b) shows the dependence of σT_C as a function of grain volume. The solid squares represent C1-C3, and open squares represent T1-T2. Each of the data points represents the average value from the thermo-remanence measurement of at least five different regions from each sample. The measured σT_C for FePt-C media C1-C3 increases significantly as the grain volume reduces and the trend is consistent with previous experimental work.[6,7] In comparison, σT_C of FePt-$BaFe_xO_y$-C media shows a 0.7% reduction in σT_C at smaller grain volume, which corresponds to around a 20% reduction compared with FePt-C media. It can be inferred that the addition of $BaFe_xO_y$ in the media layer could have an even larger effect at a smaller grain size because of the hyperbolic increase in the surface to volume ratio as the grain diameter reduces. The origin of this σT_C reduction at a smaller grain volume is the same as that causing the enhancement of M_r at elevated temperature, which was discussed above.

In summary, we have proposed the use of thermally insulating magnetic oxide materials as part of grain boundary materials in granular FePt-$L1_0$ HAMR media for suppressing the grain-to-grain T_c variation. As a practical implementation of this concept, we have conducted a systematic experimental investigation by adding $BaFe_xO_y$ in granular FePt-C HAMR media. This study shows that co-sputtered $BaFe_xO_y$ remains with the carbon in the grain boundaries and the resulting microstructures are similar to those of the FePt-C media. Moreover, the oxide in the grain boundaries forms crystalline shells, which fully surround the FePt grains surfaces. The room temperature hysteresis measurements show that the perpendicular anisotropy field and coercivity are as high as those of the reference FePt-C samples, above 70 kOe and 35 kOe, respectively. The XRD measurements show highly textured FePt with similar order parameters. The saturation remanence vs. temperature curves also indicate that the effective magnetic grain volume of $BaFe_xO_y$-C grain boundary media is greater than that of the reference C grain boundary media with a similar FePt grain size below the Curie temperature. Pulsed laser pump-probe measurements show that σT_C of FePt-$BaFe_xO_y$-C media with a grain size of 6.8 nm shows around 20% reduction relative to that of FePt-C media with the same grain size.

This work was supported by the Data Storage Systems Center of Carnegie Mellon University. The authors acknowledge the use of the Materials Characterization Facility at Carnegie Mellon University supported by Grant No. MCF-677785.

[1]M. H. Kryder, E. C. Gage, T. W. Mcdaniel, W. A. Challener, R. E. Rottmayer, G. Ju, Y.-T. Hsia, and M. F. Erden, Proc. IEEE **96**(11), 1810–1835 (2008).
[2]A. Perumal, L. Zhang, Y. K. Takahashi, and K. Hono, J. Appl. Phys. **108**, 083907 (2010).
[3]J. G. Zhu and H. Li, J. Appl. Phys. **115**, 17B747 (2014).
[4]H. Li and J. G. Zhu, IEEE Trans. Magn. **49**, 3568 (2013).
[5]H. Li and J.-G. Zhu, J. Appl. Phys. **115**, 17B744 (2014).
[6]S. Pisana, S. Jain, J. W. Reiner, O. Mosendz, G. J. Parker, M. Staffaroni, O. Hellwig, and B. C. Stipe, IEEE Trans. Magn. **51**, 1 (2015).
[7]A. Chernyshov, T. Le, B. Livshitz, O. Mryasov, C. Miller, R. Acharya, and D. Treves, J. Appl. Phys. **117**, 17D111 (2015).
[8]K. Binder and D. W. Heermann, *Monte Carlo Simulation in Statistical Physics* (Springer-Verlag, Berlin, 2010).
[9]O. Hovorka, S. Devos, Q. Coopman, W. J. Fan, C. J. Aas, R. F. L. Evans, X. Chen, G. Ju, and R. W. Chantrell, Appl. Phys. Lett. **101**, 052406 (2012).
[10]M. Sharma, S. C. Kashyap, H. C. Gupta, M. C. Dimri, K. Asokan, M. Sharma, S. C. Kashyap, H. C. Gupta, and M. C. Dimri, AIP Adv. **4**, 77129 (2014).
[11]A. F. Clark, W. M. Haynes, V. A. Deason, and R. J. Trapani, Cryogenics **16**, 267 (1976).
[12]Z. Dai, H. Li, and J. Zhu, IEEE Trans. Magn. **52**, 3201504 (2016).
[13]E. Yang, D. E. Laughlin, and J. Zhu, IEEE Trans. Magn. **48**, 7 (2012).
[14]B. S. D. C. S. Varaprasad, M. Chen, Y. K. Takahashi, and K. Hono, IEEE Trans. Magn. **49**, 718 (2013).